Diagnosis of laser-target implosions by space-resolved continuum absorption x-ray spectroscopy

F. J. Marshall, J. A. Delettrez, R. Epstein, and B. Yaakobi
Laboratory for Laser Energetics, University of Rochester, 250 East River Road, Rochester, New York 14623-1299
(Received 29 November 1993)

A technique for diagnosing the core temperature kT_{core} and shell areal density ρR_{shell} of laser-imploded targets by measurement of the space-resolved, continuum x-ray emission is described in this work. An estimate of kT_{core} is obtained from a fit to the space-resolved core x-ray spectrum. Observation of absorption by the cooler surrounding shell material is used to estimate ρR_{shell}. For the x-ray emission from the core to be detected, its flux density must exceed that of the time-integrated emission from the ablation layer, making this technique particularly applicable to diagnosis of targets with low-Z ablators. In contrast to techniques that depend upon measurements of the reaction products (e.g., knock-ons, secondary-reaction products), which are limited to low shell-areal-density implosions (< 100 mg/cm^2), space-resolved continuum-absorption spectroscopy should be applicable to the diagnosis of higher shell-areal-density implosions (> 100 mg/cm^2). This technique has been successfully applied to the diagnosis of evacuated, polymer-coated, deuterated polystyrene (CD) shell implosions (surrogate-cryogenic implosions) performed with the University of Rochester's, 24-beam uv, OMEGA laser system. Space-resolved spectra of the target x-ray emission (~ 1 to ~ 6 keV) were obtained with a grazing-incidence reflection microscope, dispersed by a transmission grating. Both a high-energy tail and absorption at low energies were observed in the x-ray spectra allowing estimates of kT_{core} and ρR_{shell} to be obtained.

PACS number(s): 52.70.La, 52.50.Jm, 52.25.Nr, 07.85.+n

I. INTRODUCTION

Diagnosis of laser-imploded fusion targets has evolved in recent years to the point where many techniques are available. There are however a limited number of techniques available to diagnose the final fuel conditions. If a pure thermonuclear fuel is used, then measurements of the reaction products can yield estimates of the compressed fuel areal density and temperature [1,2]. X-ray imaging can be used to estimate the fuel density if dopants are added to the fuel, rendering emission from the imploded fuel region detectable [3]. In the case of shell targets such as cryogenic DT-filled shells, measurements of the knock-on ion spectrum can yield estimates of the fuel areal density [4]. Also, experiments have been performed with so-called "surrogate" cryogenic targets. These targets consist of fuel in the solid state but not at cryogenic temperatures such as deuterated polystyrene (CD) shells. Measurements of final fuel areal density were obtained by measuring the number of activated Si nuclei in implosions of CDTSi shells by the "radchem" technique [5].

In this paper we describe a technique for measuring the broadband continuum spectrum of x rays emitted by imploded shell targets and the application of this technique to diagnosing the compressed shell temperature and areal density. Application of this technique to implosions of evacuated CD shells yields measurements of the core temperature and surrounding fuel areal density at approximately the time of peak compression without the need to add a higher-Z tracer element.

A previous paper introduced the concept of using measurements of core continuum radiation and shell absorption to diagnose laser compressed shells [6]. In that paper it was shown that observation of a peak in the continuum emission (in the case of gas-filled plastic shells) could be used to estimate the quantity $(\rho^2 R)_{shell}/T^{1/2}$, where ρ is the shell density, R is the shell thickness, and T is the shell temperature. In this paper we generalize this analysis of the absorption physics and show how the quantities kT_{core} and ρR_{shell} can be separately determined. This is accomplished by fitting the observed spectrum to an exponential (thermal bremsstrahlung or recombination radiation source) with absorption by the surrounding colder shell material. We further show how imaging increases the observability of such an effect.

Implosion experiments were performed on evacuated, polymer-coated CD shells with the OMEGA laser system, and spectrally dispersed x-ray images were obtained with a Kirkpatrick-Baez (KB) microscope dispersed by a transmission grating. Example spectra obtained from CD shell implosion experiments are given in this paper along with results of spectral analysis that determine estimates of kT_{core} and ρR_{shell}.

II. SPECTRALLY DISPERSED X-RAY IMAGING WITH A KIRKPATRICK-BAEZ MICROSCOPE

If modest spectral resolution is sufficient, then spectral dispersion of x rays can be efficiently obtained with transmission-grating diffraction. It was first recognized in the field of x-ray astronomy that slitless spectra of celestial sources could be obtained by using transmission gratings in conjunction with an x-ray telescope [7]. Ceglio, Hawryluk, and Price [8] extended the use of this technique to laser fusion by incorporating a transmission

grating into a Wolter type-I x-ray microscope. However, both good spatial and spectral resolution could not be simultaneously obtained. As noted by Ceglio, Hawryluk, and Price and later confirmed in experiments performed with the OMEGA laser system [9], a Kirkpatrick-Baez microscope can be used to obtain spectrally dispersed x-ray images without the necessity for compromising either spatial or spectral resolution. We have incorporated a state-of-the-art transmission grating (2000-Å period) [10] into a KB microscope with good spatial resolution (~ 5 μm), sensitivity ($\sim 3\times 10^{-7}$ sr), and large energy-bandwidth (~ 1 to ~ 7 keV). This instrument is capable of spatially resolving the broadband x-ray spectra of laser-imploded targets with sensitivity much higher than that of other methods, enabling diagnosis of the conditions in the compressed high-temperature, high-density, plasma core and its surrounding colder shell region. The detailed response of this grating-dispersed x-ray microscope is described below.

A. Imaging characteristics of Kirkpatrick-Baez microscopes

A Kirkpatrick-Baez microscope [11] consists of crossed cylindrical mirrors of width Δt. They are placed at a mean distance p from a source of x rays. The focusing geometry is shown in Fig. 1(a). The source-to-mirror distance p and the mirror-to-image distance q are related by the focus equation

$$\frac{1}{p}+\frac{1}{q}=\frac{2}{R\sin i}\ , \tag{1}$$

where R is the radius of curvature of the mirror and i is the angle the ray from P to C makes with the tangent to the mirror at C. When two perpendicular mirrors are used to obtain imaging in both dimensions, the focusing condition for each mirror is only approximately satisfied. Equation (1) still holds with p, q, and i representing average values for the mirror assembly. The resolution of the OMEGA KB microscopes has been measured in the laboratory with a cw x-ray source and found to be ~ 5 μm at optimum focus [12]. The field of view and depth of field are approximately 500 and 1000 μm, respectively. These microscopes consist of two pairs of mirrors arranged perpendicularly to each other so as to produce four images [Fig. 1(b)]. Different filters can be placed at the four image centers so as to obtain images with different energy bands and consequently different exposure levels when film is used to record the images of a laser target.

The effective solid angle of the two-mirror combination, $\Delta\Omega$, is given by

$$\Delta\Omega=\left[\frac{(\Delta t)(\sin i)}{p}\right]^2 . \tag{2}$$

The efficiency of the KB microscope is given by the product of the reflectivity of each mirror. Under the simplifying assumption of equal grazing angles and unpolarized incident radiation, the efficiency is

$$\varepsilon_{\mathrm{KB}}=[R_{\mathrm{unp}}(Z,i,E)]^2\ , \tag{3}$$

where R_{unp} is the reflectivity of a single mirror when unpolarized x rays are incident, Z is the atomic number of the coating, and E is the photon energy. The calculated mirror efficiency is shown in Fig. 2 for an assumed grazing angle of 0.70° and the constants of Henke, Guillkson, and Davis [13] for both Ni- and Au-coated mirrors. [Results in this work are solely from Au-coated mirrors. Past imaging results were obtained with Ni-coated mirrors [9,12] and hence were limited to energies below ~ 5 keV. With the increase in high-energy response afforded by the Au-coated mirrors, the high-energy limit has been increased to ~ 7 keV (Fig. 2).] A more accurate value of the calculated mirror efficiency can be obtained, if desired, by ray tracing the imaging configuration. Equation (3) is sufficiently accurate for the small solid angles being considered ($\Delta\Omega\sim 3\times 10^{-7}$ sr).

B. Grating-dispersed microscope response

To obtain a spectrally dispersed image of the target emission, a grating is placed behind the mirrors. This is conveniently placed at the baffle, where reflected x rays are passing through the symmetry axis of the microscope [Fig. 1(b)]. Zero-order (undiffracted) and first-order (diffracted) image of the target emission are obtained at the image plane. The x rays are dispersed according to

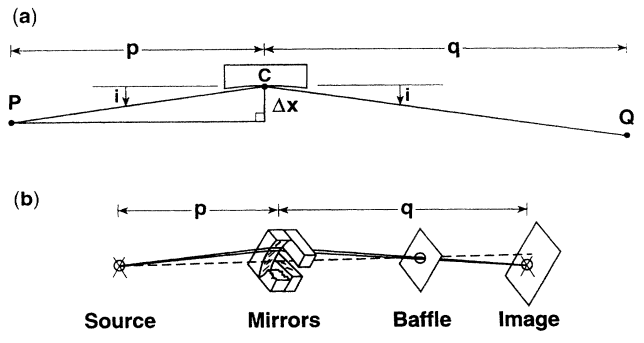

FIG. 1. Schematic of a Kirkpatrick-Baez microscope. (a) The focusing arrangement for a single mirror. (b) The arrangement of the OMEGA KB microscope crossed mirror pairs, with only one of four images shown. The microscope is spectrally dispersed by placing a transmission grating at the baffle.

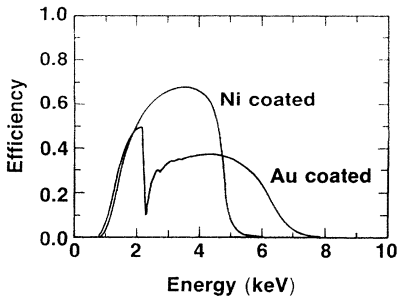

FIG. 2. Calculated efficiency of the OMEGA KB microscopes for both Au- and Ni-coated mirrors. The dip in the reflection efficiency of Au at 2.2 keV is due to the increase in the absorption of x rays by M-shell electrons (2.2 keV is the M_V edge).

the grating equation

$$n\lambda = d_g \sin\theta \ , \tag{4}$$

where n is the diffraction order, λ is the wavelength, d_g is the grating spacing, and θ is the diffraction angle. Considering first-order diffraction only ($n=1$), and with distance from the undiffracted direction being x, this can be approximated as

$$\lambda \approx \left[\frac{d_g}{D_g}\right] x \ , \tag{5}$$

where D_g is the distance from the grating to the image plane. The quantity d_g/D_g is the dispersion power of the grating. With $d_g = 2000$ Å and $D_g = 1997.3$ mm (used in the Au-coated KB microscope) the dispersion power is 1.0014 Å/mm.

Since the microscope is used to obtain a magnified image of the laser-target emission, we note that the flux detected at the image plane $f(x',y')$ is related to the surface emissivity of the target $s(x,y)$ by

$$f(x',y') = s(x,y)\frac{\Delta\Omega}{4\pi M^2}(\varepsilon_{\rm KB} T_f) \ . \tag{6}$$

where $\Delta\Omega$ is the solid angle subtended by the microscope, M is the magnification of the image, $\varepsilon_{\rm KB}$ is the efficiency of the microscope, and T_f is the transmission of all filters. (Distances in the image are magnified by the amount $M = x'/x = y'/y$.) When a grating is used to obtain dispersion, the differential flux, $df/d\lambda$ or df/dE, is observed. This is related to the observed intensity by differentiating Eq. (6) and including the grating diffraction efficiency ε_g:

$$\frac{df}{dE} = \frac{ds}{dE}\frac{\Delta\Omega}{4\pi M^2}(\varepsilon_{\rm KB}\varepsilon_g T_f) \ . \tag{7}$$

The efficiency $\varepsilon = \varepsilon_{\rm KB}\varepsilon_g T_f$ of a KB microscope dispersed by a transmission grating is shown in Fig. 3,

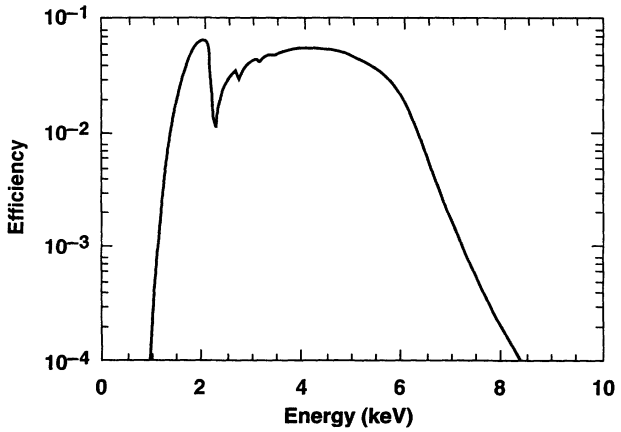

FIG. 3. Calculated efficiency of an OMEGA KB microscope with Au-coated mirrors, dispersed by a transmission grating. The calculated attenuation by a 50-μm Be filter has been included, since a 25-μm Be blast shield and a 25-μm Be film light shield are used in actual experiments. (Again, the dips in the efficiency at 2.2 keV and above are due to the effect of M-shell electrons on the efficiency.)

calculated again using the constants of Henke, Guillkson, and Davis. The efficiency includes transmission through a nominal filter T_f. (We assume that the grating acts like an ideal diffractor. Schattenburg *et al.* [10] have found that, with the exception of an energy-independent factor of order unity, the gratings made by their technique follow this ideal response. The factor arises from areas of the grating that do not diffract x rays as a result of manufacturing imperfections.) Finally we can obtain an expression that relates the observed differential dispersed flux df/dx to the target surface flux density ds/dE. By using the relation $E = hc/\lambda$ in Eq. (5), diferentiating both sides, substituting this into Eq. (7), and solving for ds/dE, we obtain

$$\frac{ds}{dE} = -\frac{hc}{E^2}\frac{D_g}{d_g}\frac{4\pi M^2}{\Delta\Omega}\frac{df/dx}{(\varepsilon_{\rm KB}\varepsilon_g T_f)} \ . \tag{8}$$

The minus sign in Eq. (8) arises from the fact that increasing energy is in the direction of decreasing dispersion distance.

C. Analysis of grating-dispersed images

Intense radiation is emitted from the center of an imploded shell target. The emission comes from a hot, dense plasma, which results when the imploding shell stagnates. The radiation then passes through the lower temperature region surrounding the central hot spot and undergoes partial absorption in this layer. The emergent radiation can be represented by the integral form of the radiation transport equation

$$I(E) = \int_{-\infty}^{\infty} j(E,s)\exp[-\tau(E,s)]ds \ , \tag{9a}$$

$$\tau(E,s) = \int_{S}^{\infty} \kappa(E,s')ds' \ , \tag{9b}$$

where $j(E,s)$ is the emissivity at energy E and position s along a path through the emitting region, τ is the optical depth, and κ is the opacity. A simplification arises if it is assumed that all of the radiation emanates from the origin (core). Then Eq. (9a) can be rewritten as

$$I(E) = I_{\rm core}(E)\exp[-\tau(E)] \ , \tag{10a}$$

$$\tau(E) = \int_{0}^{\infty} \kappa(E,r)dr \ , \tag{10b}$$

where $I_{\rm core}(E)$ is the flux density of the core emission in keV/keV/cm^2.

The optical depth τ is proportional to the areal density $\langle \rho R \rangle$ since Eq. (10b) can be expressed in terms of the mass absorption coefficient $\mu = \kappa/\rho$ as follows:

$$\tau(E) = \int_{0}^{\infty} \mu(E,r)\rho\, dr \tag{11a}$$

$$= \langle \mu(E) \rangle \langle \rho R \rangle \ , \tag{11b}$$

where

$$\langle \mu(E) \rangle \equiv \int_{0}^{\infty} \mu\rho\, dr / \langle \rho R \rangle \tag{11c}$$

and

$$\langle \rho R \rangle \equiv \int_{0}^{\infty} \rho\, dr \ . \tag{11d}$$

The optical depth is therefore equal to the product of the density-averaged mass-absorption coefficient times the areal density.

Actual implosions do not result in a pointlike emission region and are observed with finite spatial resolution. The resulting flux distribution observed by a grating-dispersed microscope is described by a convolution between space and spectrum. The observed flux is given by

$$F(x,y,\lambda)=\int \frac{dF}{dx'}(x-x',y,\lambda)\varepsilon(x')dx' , \tag{12}$$

where $x'=c_g\lambda$, $c_g=D_g/d_g$, and $\varepsilon=\varepsilon_{KB}\varepsilon_g T_f$ is the dispersed microscope sensitivity. If it is assumed that the spectrum of the emission varies little from its average over the core region and it is confined to a finite region, then

$$\frac{dF}{dx'}\approx\frac{df(\lambda)}{dx}i(x-x',y) , \tag{13}$$

where $i(x,y)$ is the unitless flux density versus position (i.e., the shape of the emission region). The function $df(\lambda)/dx$ is treated as a constant in the integration, and we arrive at the expression for the observed differential flux

$$\frac{df(\lambda)}{dx}=F(x,y,\lambda)\Big/\int i(x-x',y)\varepsilon(x')dx' . \tag{14}$$

In practice, the laser-target implosions are sufficiently symmetric that the core size can be measured accurately from the undispersed direction of the grating-dispersed image. This information is then used to compute the convolution integral in Eq. (14). The effect of the finite source size is to blur the spectral resolution of the grating-dispersed microscope, as shown in Fig. 4. The solid line is the computed efficiency of the grating-dispersed microscope versus wavelength for a point source. The dotted line in Fig. 4 shows the computed response to a source of size 15 μm in radius when the grating dispersion was 1.0014 Å/mm (as was the case for the results given in this paper). The effect is to average (convolve) the response versus wavelength over surrounding wavelengths.

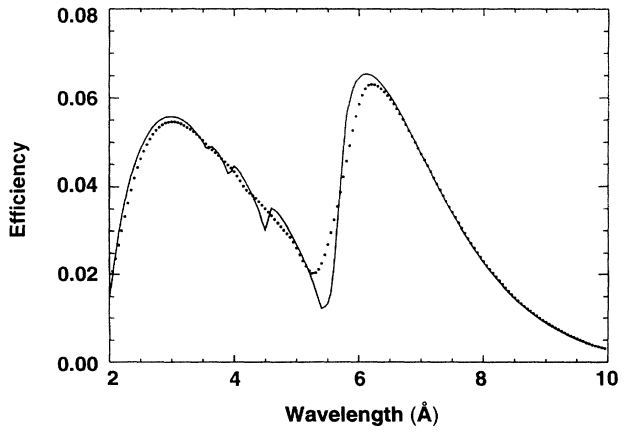

FIG. 4. Calculated efficiency versus wavelength of the grating-dispersed microscope for a point source (solid line). The dotted line is the convolved response versus wavelength (or equivalently position) for a finite-sized source (15 μm in radius for this case).

III. CONTINUUM ABSORPTION BY THE IMPLODED LASER TARGET

The absorption of x rays by the plasma surrounding the hot, dense core of an imploded laser target is principally by bound-free and free-free absorption processes. The absorption by free electrons in the plasma has an opacity κ_{ff} given by [14]

$$\kappa_{ff}=\frac{3.68\times10^{8}}{\nu^3T^{1/2}}N_e\sum_i N_iZ_i^2 \text{ cm}^{-1} , \tag{15}$$

where ν is the frequency in Hz, T is the temperature in kelvin, N_e is the electron density, and N_i is the density of the ion species whose charge is Z_i. For the case of a neutral plasma,

$$\kappa_{ff}=\frac{3.68\times10^{8}}{M^2}\frac{\rho^2}{\nu^3T^{1/2}}\langle Z^2\rangle\langle Z\rangle , \tag{16}$$

where M is the average ion mass and ρ is the mass density. For a CD plasma, $\langle Z^2\rangle=18.5$, $\langle Z\rangle=3.5$, and $M=7m_p$, where m_p is the mass of the proton. The expression for the opacity reduces to

$$\kappa_{ff}(\text{CD})=\frac{3.61\rho^2}{E^3(kT)^{1/2}} \text{ cm}^{-1} , \tag{17}$$

where E is the photon energy in keV and kT is the temperature in keV.

For the case of incomplete ionization, significant absorption will take place due to photoionization of the remaining bound electrons. If the number density of each ionic species is determined and the photoelectric absorption cross section per ion is known, then the opacity of the medium can be determined. The bound-free cross section per k-shell electron (the dominant contributors to absorption) for an ion whose nuclear charge is Z is given by [15]

$$\sigma_{bf}=2.12\times10^{-23}Z_{\text{eff}}^4\frac{1}{E^3} \text{ cm}^2/\text{electron} , \tag{18}$$

where E is in keV, $Z_{\text{eff}}=Z-s$, and s is the Slater screening constant. For hydrogenlike ions $s=0$, and for heliumlike and higher $s=0.3$. For carbon ions the result is $\sigma_{bf}(C^{5+})=2.75\times10^{-20}E^{-3}$ cm^2 and $\sigma_{bf}(C^{4+})=2.24\times10^{-20}E^{-3}$ cm^2, where E is in keV. If the species are assumed to be in local thermodynamic equilibrium, then the number density of each species can be determined from the Saha equation

$$\frac{N_{r+1}N_e}{N_r}=\left[\frac{g_{r+1}}{g_r}\right]\frac{2(2\pi m_ekT)^{3/2}}{h^3}\exp(-I_r/kT) , \tag{19}$$

where the subscript r refers to the charge of the remaining ion and I_r is the ionization potential. The bound-free opacity of a CD plasma can be accurately approximated by the opacity of the hydrogenlike and heliumlike carbon ions, yielding

$$\kappa_{bf}(\mathrm{CD}) \approx N_{C^{4+}} \sigma_{bf}(C^{4+}) + N_{C^{5+}} \sigma_{bf}(C^{5+}) . \quad (20)$$

Reexpressing the opacity in terms of the mass density (using $\rho = 2MN_c$ and assuming $N_C \simeq N_{C^{4+}} + N_{C^{5+}} + N_{C^{6+}}$), Eq. (20) can be written as

$$\kappa_{bf}(\mathrm{CD}) = \frac{\rho \sigma_{bf}(C^{4+})}{2M} \frac{N_{C^{4+}}}{N_C} \left[1 + \alpha \frac{N_{C^{5+}}}{N_{C^{4+}}} \right] , \quad (21)$$

where $\alpha = \sigma_{bf}(C^{5+})/\sigma_{bf}(C^{4+})$. Taking into account the fact that the heliumlike ion has two electrons, $\alpha = 0.614$. Using the Saha equation to determine the ratio of the components and with $g_4 = 1$, $g_5 = 2$, $g_6 = 1$, $I_4 = 0.392$ keV, $I_5 = 0.490$ keV, $N_e = \langle Z \rangle \rho / M$, we obtain

$$\kappa_{bf} = 1.91 \times 10^3 \frac{\rho}{E^3} f(\rho, kT) , \quad (22)$$

where

$$f(\rho, kT) = \frac{\left[1 + 0.614 \times \frac{1.278 \times 10^3}{\rho} (kT)^{3/2} e^{-0.392/kT} \right]}{\left[1 + \frac{1.278 \times 10^3 (kT)^{3/2}}{\rho} e^{-0.392/kT} + \frac{4.083 \times 10^5 (kT)^3}{\rho^2} e^{-0.882/kT} \right]} .$$

The ratio of the bound-free and free-free components of the photoelectric absorption cross section, κ_{bf}/κ_{ff}, is given by

$$\frac{\kappa_{bf}}{\kappa_{ff}} = \frac{529}{\rho} \sqrt{kT} f(\rho, kT) . \quad (23)$$

The expression for κ_{ff} was derived under the assumption of complete ionization. This will be a slight overestimate if an appreciable fraction of the carbon ions are not completely ionized. The ratio κ_{bf}/κ_{ff} is plotted in Fig. 5 versus temperature for values of density ranging from 0.1 to 100 g/cm^3. The bound-free absorption is seen to dominate for $\rho \lesssim 10^2$ and $kT \lesssim 0.5$ keV. The total mass absorption coefficient $\mu = \mu_{bf} + \mu_{ff}$ is given by

$$\mu = 1.91 \times 10^3 \frac{1}{E^3} g(\rho, kT) , \quad (24)$$

where

$$g(\rho, kT) = f(\rho, kT) + \frac{\rho}{529\sqrt{kT}} .$$

The total mass absorption coefficient times E^3 (which is equivalent to its value at 1 keV) is plotted in Fig. 6 versus temperature for different values of density. It can be seen that μE^3 is constant for low densities and low temperatures but decreases with increasing temperature and increases with increasing density. Of relevance to the absorption of core radiation and for $\rho \lesssim 10^2$, the dominant fraction of the absorption will occur in regions where the temperature is $\lesssim 200$ eV, if they are present.

When x rays are emitted by the collapsed core of a laser-imploded shell, the high-energy portion of the emission can often be characterized by a single temperature exponential spectrum. Taking into account absorption as described above, this spectrum takes the form

$$I = I_0 e^{-E/kT_{\mathrm{core}}} e^{-\mu \rho R} , \quad (25)$$

where T_{core} is the temperature of the emitting plasma, and μ and ρR are assumed to be averaged over the shell [e.g., Eqs. (11c)–(11d)]. (For evacuated shell targets, $\rho R \simeq \rho R_{\mathrm{shell}}$, which is assumed in the remainder of this work.)

As noted by Yaakobi, Epstein, and Marshall [6] this spectrum has a peak at an energy $E_{\max}$ given by

$$\frac{E_{\max}}{E_1} = \left[\frac{3kT_{\mathrm{core}}}{E_1} \right]^{1/4} , \quad (26)$$

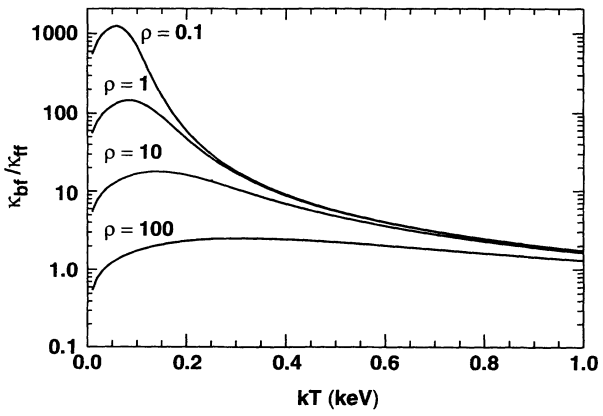

FIG. 5. Ratio of bound-free to free-free absorption in a CD plasma versus temperature for densities of 0.1, 1, 10, and 100 g/cm^3.

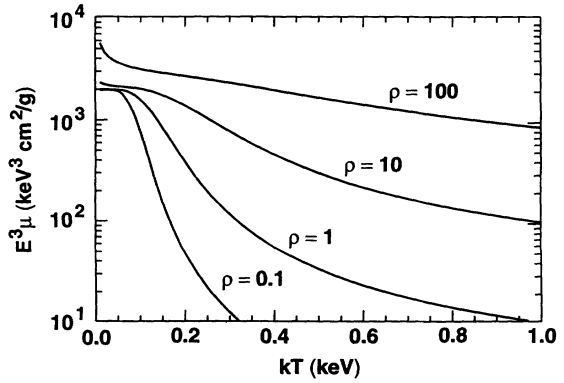

FIG. 6. Total mass absorption coefficient μ (times E^3) of a CD plasma versus temperature for densities of 0.1, 1, 10, and 100 g/cm^3.

and where we find for CD,

$$E_1=[1.91\times10^3 g(\rho,kT)\rho R]^{1/3} . \quad (27)$$

Fitting of the observed spectrum to the form of Eq. (25) can more accurately determine both of the important parameters kT_{core} and ρR.

Once the opacity is determined by a functional fit to the data, then in the case of $kT \lesssim 100$ eV $\rho \lesssim 10$ g/cm^3, ρR can be approximated by

$$\rho R \approx \tau_1/1.91\times10^3 \text{ g/cm}^2 , \quad (28)$$

where τ_1 is the equivalent opacity at 1 keV. This amounts to equating the opacity to that of neutral carbon in the CD material. [We note that this simple model asymptotically agrees at $kT=0$ with the value calculated from neutral carbon opacities [13] averaged over the energies of interest here (2 to 6 keV).] Provided that the free-free absorption is not significant, we can therefore determine a conservative lower limit to the value of ρR by assuming that the opacity is that of neutral matter. A more exact determination of ρR would require additional knowledge of conditions in the absorbing region.

In the higher-density case ($\rho \gtrsim 10^2$ g/cm^3),

$$\rho^2 R = 0.277\tau_1\sqrt{kT} \text{ g}^2/\text{cm}^5 , \quad (29)$$

requiring independent knowledge of the density and temperature in order to determine ρR. We can, however, relate τ_1 to ρR more directly. In the idealized case where the shell has been compressed to a uniform sphere and the flux comes from a hot spot at the center, mass conservation yields

$$\rho = \sqrt{4\pi/3M_a}(\rho R)^{3/2} , \quad (30)$$

where M_a is the mass of the absorbing (shell) material. Substituting for ρ in Eq. (29) yields

$$\tau_1 = 3.61\sqrt{4\pi/3M_a kT}\,(\rho R)^{5/2} \quad (31)$$

or

$$\rho R = \left[\frac{\tau_1}{3.61}\right]^{2/5}\left[\frac{3M_a kT}{4\pi}\right]^{1/5} \text{g/cm}^2 . \quad (32)$$

Strictly speaking, the product $M_a kT$ must be known to apply Eq. (32). However, since it appears to the one-fifth power, even a factor-of-2 error in the assumed value will lead to only a 13% error in the derived value of ρR. In practice, a reasonable estimate of $M_a kT$ should be obtainable from hydrocode simulations, thereby not contributing appreciably to error in the derived value of ρR. [We note that at extreme densities ($\rho \gtrsim 3\times10^2$ g/cm^3) the electrons will be partly degenerate and Eq. (15) will no longer be valid. We have not attempted to address that case in this work.]

At this point it is worth asking: With the above considerations, what conditions are necessary in order that a spectral signature of shell absorption be observed? Most apparent is that the implosion must result in a centrally peaked hot spot that generates sufficiently high energy x-ray emission to be detectable. Implosions of hollow targets by their nature tend to satisfy this condition since there is an effective conversion of kinetic energy into thermal energy upon void closure. (Yaakobi, Epstein, and Marshall [6] found this technique applicable to gas-filled shell implosions as well.) Secondly, the peak and tail of the core emission spectrum must be detected in order to fit the parameters kT_{core} and ρR_{shell}. The maximum measurable ρR_{shell} is limited to values that produce a peak within the sensitive range of the imaging device. As an example, for $kT=1$ keV and $\rho R=100$ mg/cm^2, using Eq. (27) and assuming $g(\rho,kT)\approx1$, we find $E_{\max}=4.9$ keV. For the same conditions and $\rho R=200$ mg/cm^2, we find $E_{\max}=5.8$ keV. In these examples the peak in the spectrum would fall within the sensitive range of the grating-dispersed x-ray microscope used in this work. Higher ρR values could be measured provided an instrument with appropriate high-energy sensitivity is used.

IV. SIMULATIONS OF HOLLOW-SHELL-TARGET IMPLOSIONS

It can be shown [16] that the parameters of a hollow-shell or "surrogate-cryogenic" target can be chosen such that its implosion is hydrodynamically similar to that of an actual cryogenic target (e.g., solid DT filled). The assumption therefore is that the study of the implosion of such targets will add to the understanding of actual cryogenic-target implosions. Simulations have been performed with the hydrodynamics code LILAC. Assumptions used in the simulations are the same as those given by Marshall *et al.* [4]. Of interest to this work is the predicted total and core x-ray emission spectrum from a surrogate-cryogenic-target implosion. Figure 7 shows details of the predicted time-integrated and space-integrated spectrum from one such simulation (curve marked total). The assumed conditions are 1400 J of uv (351 nm) on target, 600-ps pulse width [full width at half maximum (FWHM)], 114-μm inner radius evacuated CD shell, 4.0 μm thick with a 6.0-μm parylene (CH) overcoat to act as an ablation layer. The flux emitted within particular radial regions are also shown for radii of 5 μm, 10 μm, and 50 μm. The high-energy flux, with a peak at $\sim$5 keV, is apparently from the inner $\sim$5 μm of the implo-

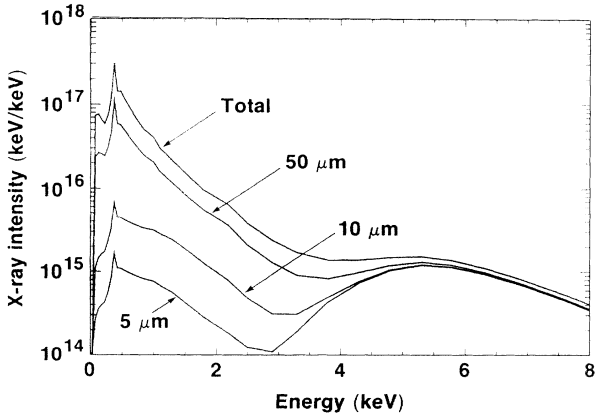

FIG. 7. LILAC-predicted x-ray spectrum of a CD-shell implosion, integrated over regions extending to radii of 5 μm, 10 μm, and 50 μm from the implosion center, and integrated over space (total).

sion core. When the high-energy portion of this spectrum is fitted to Eq. (25) and assuming the cold, low-density mass absorption coefficient given by Eq. (24) with $g(\rho,kT)\approx 1$, the resulting values are $kT_{\text{core}}=1.26$ keV and $\rho R=0.106$ g/cm^2. This compares with the calculated peak values from the same simulation of $kT_{\text{core}}=1.54$ and $\rho R=0.199$ g/cm^2. The values determined from the simulated spectrum are lower than the actual simulated peak values, as expected, since the simulated spectrum is an average over time, over the region of the compressed shell, and since the shell material is not cold.

To summarize the results of the CD-target-implosion simulation, the high-energy flux is predicted to be principally from the implosion core, and both the central electron temperature kT_{hot}, and the surrounding shell areal density ρR can be reliably estimated from the emitted core spectrum. The observability of the high-energy core flux, in particular the peak due to absorption, is dramatically increased when imaging is employed.

V. EXPERIMENTS

A grating-dispersed KB microscope was positioned on the OMEGA target chamber. Images were recorded with DEF film, processed, and reduced by the method specified by Henke *et al.* [17]. Digitizing was accomplished with a Perkin Elmer PDS microdensitometer. The microscope was readied for a target experiment by placing a custom removable film cartridge, having a 25-μm Be x-ray window, at the image plane. The film cartridge was positioned so as to record the image from one of four corners of the optical assembly. After pump-out, an intervening gate-valve was opened to allow film exposure. The x-ray optical assembly was shielded from direct target debris by an enclosure with an additional 25-μm Be window acting as a blast shield. The focal distances p and q [see Eq. (1)] were 186.4 mm and 2200.0 mm, respectively. The grating-to-film distance was 1997.3 mm yielding a dispersion of 1.0014 Å/mm. In

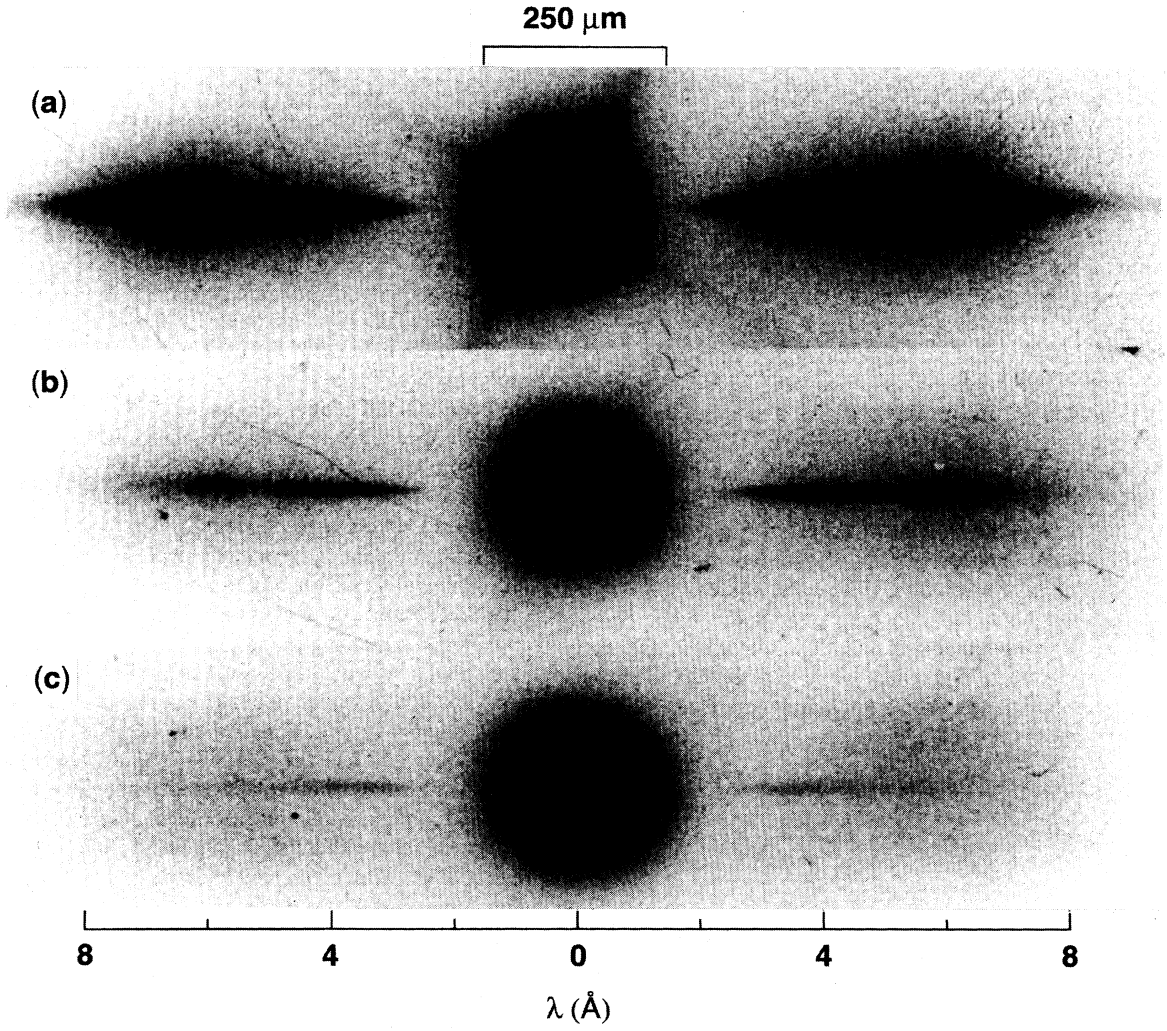

FIG. 8. Grating-dispersed KB-microscope images from a series of CD-shell target implosions for (a) 8-μm, (b) 10-μm, and (c) 12-μm-thick shells. For reference the scale of the undiffracted image is indicated in micrometers, as is the scale of the diffracted emission in angstroms.

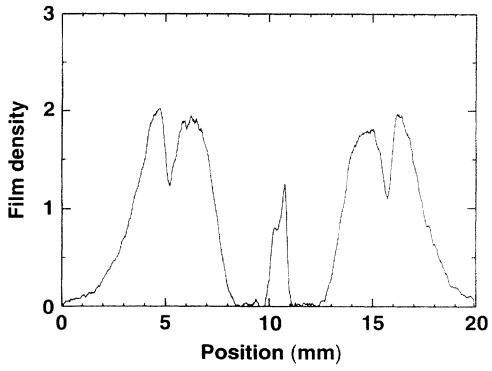

FIG. 9. Lineout through the CD-shell implosion image of Fig. 8(a).

this configuration a single corner of the KB microscope had an effective area of $\Delta\Omega = 3.9 \times 10^{-7}$ sr.

Examples of exposures obtained from a series of CD-shell target implosions are shown in Fig. 8. The targets were imploded under similar conditions: 24-beam uv illumination (351 nm), with beam smoothing by spectral dispersion [18] (SSD) at a frequency of 9 GHz, a bandwidth $\Delta\lambda/\lambda \sim 0.03\%$, ~ 1150 J on target, with $\sim 65\%$ absorption, and a pulse width of ~ 600 ps (FWHM). The targets consisted of evacuated CD shells, 4.0 μm thick, 125.0-μm inner radius, with (a) 4.0-μm, (b) 6.0-μm, and (c) 8.0-μm coatings of parylene to act as an ablation layer. In addition all three targets had a 500-Å (0.05-μm) Al overcoat to prevent shinethrough [19]. Although a large variation in grating-dispersed flux from the core is evident in going from Figs. 8(a) to 8(c), all three can be easily discerned. It is also evident that, without the aid of imaging, the core emission [especially in Fig. 9(c)] would not be discernible. [The spikes appearing to emanate from the center of the implosions are due to small angle scattering of x rays off of the mirrors of the KB microscope. The scattered flux is a small fraction of the specularly reflected flux ($\lesssim 1\%$). The grating was purposely oriented such that the diffraction direction was at an angle ($\sim 45°$) to the mirror planes of incidence, effectively separating the scattered and diffracted fluxes from the core.]

Figure 9 shows an example line out through the dispersed spectrum of Fig. 8(b). The plotted film density has been reduced to the dispersed core flux alone by subtracting the background, as a function of position along the spectrum, averaging from above and below the spectrum. This eliminates film fog and contributions from the undiffracted image. Both first-order peaks are seen and, noise features aside, are identical. The shape of the uncorrected lineout is dominated by the response features of the KB-microscope grating combination (see Fig. 4). The core emission spectrum is computed using Eq. (8) and corrected for film response as specified by Henke *et al.* [17]. Figure 10(a) shows the spectrum computed assuming a point source emitter. The feature at 2.2 keV is not an expected feature, rather it arises from the convolution of space and spectrum in the diffracted emission and from residual errors in knowledge of the response function at the sharp dip at 2.2 keV. The feature is approximately removed, and a more accurate emission spectrum is computed by dividing by a convolved response function [Eq. (14) and Fig. 4]. The resulting computed spectrum is shown in Fig. 10(b). The computed spectrum is seen to be nearly free of the false feature at 2.2 keV and has the shape expected from thermal bremsstrahlung emission with absorption at low energies due to a cooler intervening plasma.

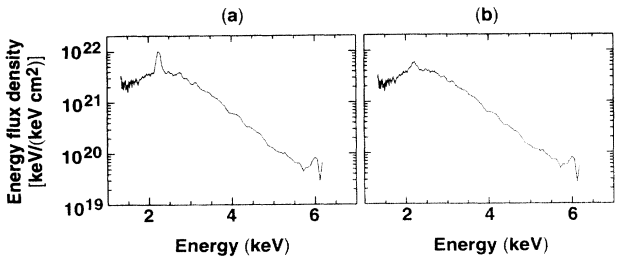

FIG. 10. Computed energy spectrum of the CD-shell implosion [from Fig. 8(a)], (a) assuming a point source emitter, and (b) the more accurate version computed by convolving the wavelength response with the source size.

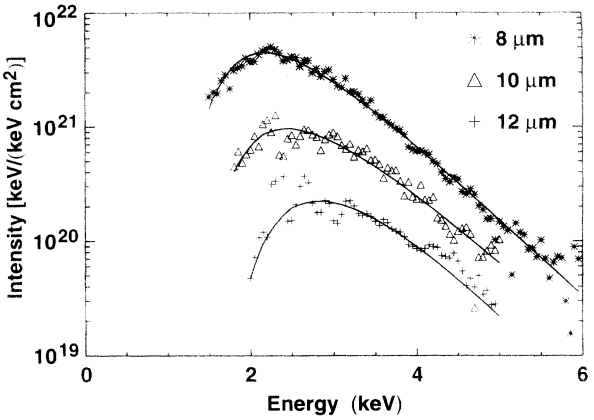

FIG. 11. Results of spectral fits to the series of CD-shell implosion spectra (Fig. 8). The measured values are shown with the indicated symbols, and the best-fit spectra are drawn as solid lines.

Figure 11 shows the result of fitting Eq. (25) to the energy spectra obtained from the series of CD-target implosions shown in Fig. 9 using the method of least squares [20]. In each case the shape of the observed spectrum is well modeled by the best-fit spectrum. The best-fit values of the important parameters were $\rho R = 5.6 \pm 1.4$, 9.2 ± 3.3, and 18.6 ± 5.0 mg/cm^2; $kT_{\text{core}} = 0.61 \pm 0.05$, 0.68 ± 0.12, and 0.60 ± 0.12 keV for the 8-, 10-, and 12-μm-thick shells, respectively. [The values of ρR were determined by assuming that Eq. (28) applies.] As was stated in Sec. III, assuming the opacity of the absorbing shell materials was that of cold matter yields a conservative value of ρR [with the provision that the density is not sufficient for free-free absorption to contribute significantly ($\rho \lesssim 10^2$)]. The above determined values of ρR then represent lower limits to the actual values of ρR that were achieved.

VI. DISCUSSION AND CONCLUSIONS

The technique of space-resolved continuum-absorption x-ray spectroscopy has been demonstrated to be a means of measuring the core electron temperature and shell areal density of laser-imploded targets. The spectrum can be obtained with a Kirkpatrick-Baez microscope, disperse by a transmission grating. Typically, the core contribution to the total emission is small and without imaging might not be discernible. With imaging, the dispersed flux from the core is concentrated into a narrow line whose dimensions are much smaller than that of the surrounding shell emission.

A review of the physics of the absorption shows that, for CD shells (and hence CH), the dominant contribution is from the bound-free process provided $\rho \lesssim 10^2$ g/cm^3 in the absorbing region. In such a case, $\tau \propto \rho R$, so a fit to the observed core spectrum can provide an estimate of ρR. Furthermore, if cold opacities are used, the determined value of ρR will be a lower limit. For $\rho > 10^2$, where free-free absorption can dominate, $\tau \propto \rho^2 R$. However, with the additional information provided by hydrocode simulations of the mass and temperature of the absorbing material, the value of ρR can still be determined. An estimate of the core electron temperature kT_{core} can be determined from the observed core spectra in either case with no need for additional assumptions.

The effects on this technique of mixing of hot core material with cold shell material is beyond the scope of this work; however, some conclusions as to its effect can be made. If the outer regions of the core mix with the shell material, this will cool that portion of the core and heat the inner shell material resulting in less emission from the core and less absorption from the shell. Nevertheless, spectroscopic diagnosis of the emission with this technique should provide a valid estimate of the reduced kT_{core} and ρR_{shell}. Any improvements to the implosion conditions that mitigate this mixing (such as improved illumination uniformity) should result in a higher observed kT_{core} and ρR_{shell}. Severe fuel-shell mixing may result in the total disruption of the implosion making it unlikely that any absorbed core x-ray spectrum would be observed. Therefore, the observation of a hot core x-ray spectrum with absorption at low energies would verify that the shell material was not severely disrupted at the time of peak compression. Partial mixing would require detailed modeling in order to properly estimate its effect on the observed spectrum.

In conclusion, we have used the technique of space-resolved continuum-absorption x-ray spectroscopy to obtain measurements of kT_{core} and ρR_{shell} at intermediate values of ρR (up to ~ 20 mg/cm^2). Furthermore, we have demonstrated that this technique should also be applicable at higher shell areal densities ($\rho R > 100$ mg/cm^2) as will be encountered in future ignition-scaling experiments.

ACKNOWLEDGMENTS

The authors acknowledge the support of the Laser Operations Group, Experimental Group, Target Fabrication Group, and staff of the Laboratory for Laser Energetics. The x-ray grating used in this work was provided by M. L. Schattenburg of the Massachusetts Institute of Technology, Center for Space Research, and the Nanostructures Laboratory. This work was supported by the U.S. Department of Energy Office of Inertial Confinement Fusion under Cooperative Agreement No. DE-FC03-92SF19460, the University of Rochester, and the New York State Energy Research and Development Authority.

[1] H. Azechi, M. D. Cable, and R. O. Stapf, Laser Part. Beams **9**, 119 (1991).
[2] H. Brysk, Plasma Phys. **15**, 611 (1973).
[3] J. D. Kilkenny, M. D. Cable, E. M. Campbell, L. W. Coleman, D. L. Correll, R. P. Drake, R. J. Ellis, S. G. Glendinning, C. W. Hatcher, S. P. Hatchett, J. P. Hunt, D. R. Kania, R. L. Kauffman, H. N. Kornblum, D. T. Kyrazis, S. M. Lane, R. A. Lerche, J. D. Lindl, W. H. Lowdermilk, D. H. Munro, D. W. Phillion, D. B. Ress, D. R. Speck, E. Storm, L. J. Suter, G. L Tietbohl, A. R. Thiessen, R. S. Thoe, R. E. Turner, J. D. Wiedwald, and F. Ze, in *Plasma Physics and Controlled Nuclear Fusion Research-1988* (IAEA, Vienna, 1989), Vol. 3, pp. 29–41.
[4] F. J. Marshall, S. A. Letzring, C. P. Verdon, S. Skupsky, R. L. Keck, J. P. Knauer, R. L. Kremens, D. K. Bradley, T. Kessler, J. Delettrez, H. Kim, J. M. Soures, and R. L. McCrory, Phys. Rev. A **40**, 2547 (1989).
[5] S. Nakai, ILE Quarterly Progress Report No. ILE-QPR-89-29, 1989 (unpublished), pp. 9–18.
[6] B. Yaakobi, R. Epstein, and F. J. Marshall, Phys. Rev. A **44**, 8429 (1991).
[7] H. Gursky and T. Zehnpfenning, Appl. Opt. **5**, 875 (1966).
[8] N. M. Ceglio, A. M. Hawryluk, and R. H. Price, Appl. Opt. **21**, 3953 (1982).
[9] M. C. Richardson, R. S. Marjoribanks, S. A. Letzring, J. M. Forsyth, and D. M. Villeneuve, IEEE J. Quantum Electron. **QE-19**, 1861 (1983).
[10] M. L. Schattenburg, C. R. Canizares, D. Dewey, K. A. Flanagan, M. A. Hamnett, A. M. Levine, S. K. Lum, R. Manikkalingam, T. H. Markert, and H. I. Smith, Opt. Eng. **30**, 1590 (1991).
[11] P. Kirkpatrick and A. V. Baez, J. Opt. Soc. Am. **38**, 766 (1948).
[12] Laboratory for Laser Energetics LLE Review **46**, Quarterly Report No. DOE/DP40200-156, 91–98 (1991) (unpublished).
[13] B. L. Henke, E. M. Gullikson, and J. C. Davis, At. Data Nucl. Data Tables **54**, 181 (1993).
[14] Ya. B. Zel-dovich and Yu. P. Raiser, *Physics of Shock Waves and High Temperature Hydrodynamic Phenomena,* edited by W. D. Hayes and R. F. Probstein (Academic, New York, 1966), Vol. 1, pp. 269–272.
[15] H. A. Bethe and E. E. Salpeter, *Quantum Mechanics of One- and Two-electron Atoms* (Academic, New York, 1957), pp. 295–305.
[16] C. P. Verdon (private communication).

[17] B. L. Henke, J. Y. Uejio, G. F. Stone, C. H. Dittmore, and F. G. Fujiwara, J. Opt. Soc. Am. B **3**, 1540 (1986).

[18] R. W. Short, T. J. Kessler, R. S. Craxton, S. A. Letzring, and J. M. Soures, J. Appl. Phys. **66**, 3456 (1989); and Laboratory for Laser Energetics Report No. 200, 1989 (unpublished).

[19] D. K. Bradley, T. R. Boehly, D. L. Brown, J. A. Delettrez, W. Seka, and D. J. Smith, in *Laser Interaction and Related Plasma Phenomena,* edited by H. Hora and G. H. Miley (Plenum, New York, 1991), Vol. 9, pp. 323–334.

[20] P. R. Bevington, *Data Reduction and Error Analysis for the Physical Sciences* (McGraw-Hill, New York, 1969), pp. 232–246.

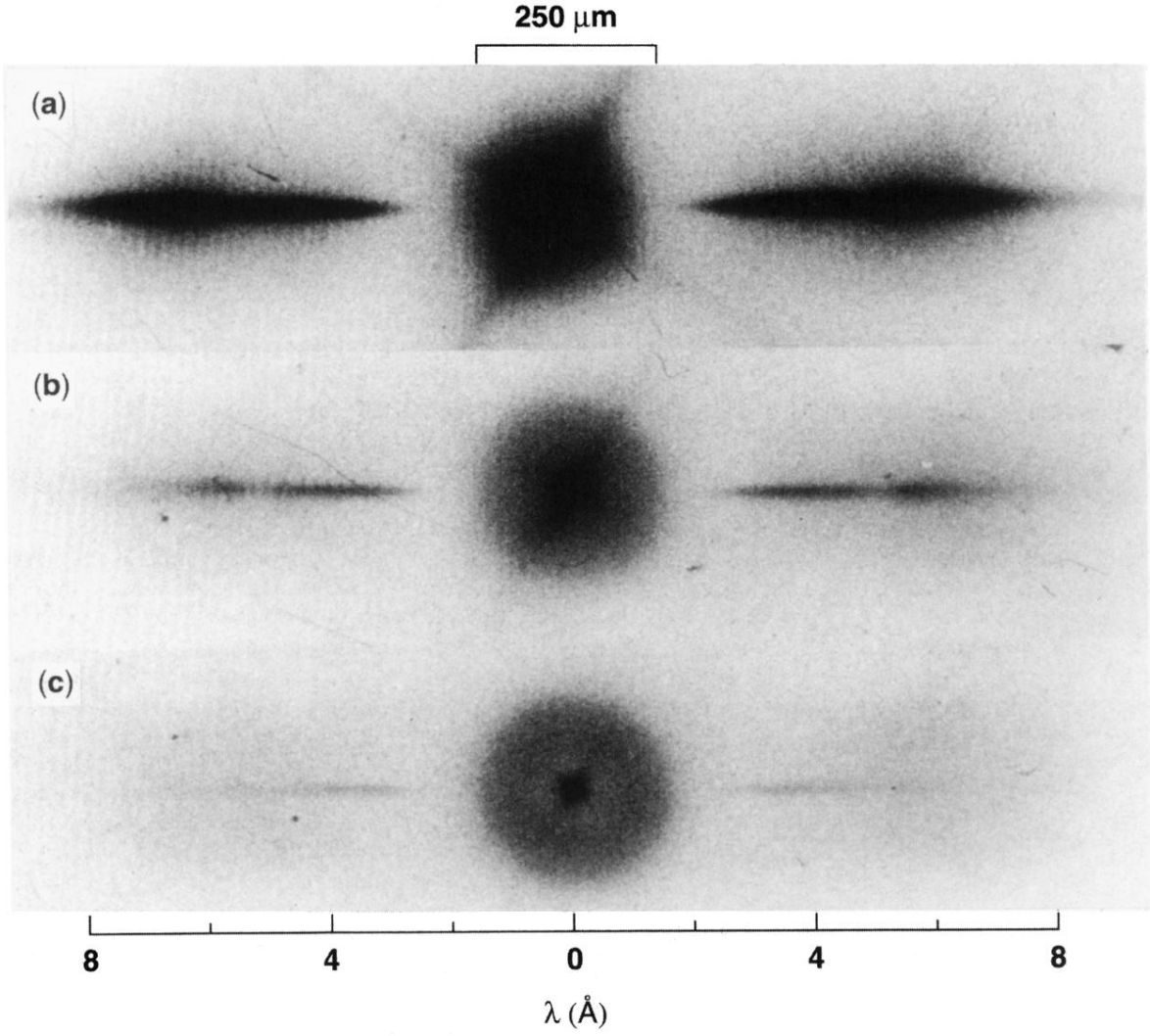

FIG. 8. Grating-dispersed KB-microscope images from a series of CD-shell target implosions for (a) 8-μm, (b) 10-μm, and (c) 12-μm-thick shells. For reference the scale of the undiffracted image is indicated in micrometers, as is the scale of the diffracted emission in angstroms.